The innate immune response against mycobacterial infection : analysis by a combination of light and electron microscopy

Hosseini, R.

CHAPTER 3

DYNAMIC INTERACTION BETWEEN LEUKOCYTES DETERMINES THE PROGRESSION OF INFECTION DURING EARLY MYCOBACTERIAL PATHOGENESIS

Rohola Hosseini, Gerda E. M. Lamers, Hiwa M. Soltani, Annemarie H. Meijer, Herman P. Spaink, Marcel J. M. Schaaf

Submitted

Abstract

Macrophages and neutrophils are the first cellular responders against invading pathogens and contribute strongly to the host defense against intracellular pathogens. The collective interplay and dynamic interactions between these leukocytes are to a large extent uncomprehended, and in the present study we have investigated their role using a combination of confocal laser scanning and electron microscopy in a zebrafish model for tuberculosis, a local *Mycobacterium marinum* (*Mm*) infection in the tail fin. Our results show that neutrophils are efficient in phagocytosis of *Mm* and that they contribute largely to the dissemination of bacteria. Macrophages appear to play a major role in efferocytosis, phagocytosis of dead cells that contain bacterial content. Eventually, large bacterial aggregates inside phagocytic cells are formed due to continuous efferocytosis, and they can be extruded out of the tail fin. Alternatively, the macrophages containing these aggregates may undergo burst. Thus, here we show the specific key functions of macrophages and neutrophils during the progression of early *Mm* infection.

Introduction

Macrophages and neutrophils are the first cells responding to invading pathogens, and during the early stages of mycobacterial infection they are the main cell types to be infected (Silva et al., 1989; Eum et al., 2010). Although macrophages are the main cell type associated with mycobacterial infection, a growing body of evidence is showing that other phagocytic cells play a major role during mycobacterial infection as well (Berry et al., 2010; Nouailles et al., 2014; Srivastava et al., 2014; Eum et al., 2010). Especially neutrophils, which are often the first responders in the host defense towards invading pathogens, appear to play a crucial protective role during a mycobacterial infection, for example by producing reactive oxygen and nitrogen species (Elks et al., 2013; Yang et al., 2008; 2012). However, how macrophages and neutrophils collectively interplay and their specific dynamic interactions during the host response against intracellular pathogens is still unclear. The present study focuses on the quantification and high resolution imaging of macrophage and neutrophil function and dynamics and during mycobacterial infection. This is required for the understanding of the specific role of infected macrophages and neutrophils play during infection and their distinct contribution to the host-defense and bacterial dissemination.

Studying the early stages of mycobacterial infections in zebrafish has been an effective approach to study host-pathogen interactions. In the present study, we have used the fish pathogen *M. marinum* (*Mm*), a close relative of *M. tuberculosis* (*Mtb*), the causative agent of tuberculosis in humans, to investigate the complex dynamic response of leukocytes towards mycobacterial infection. *Mm* displays a similar pathogenesis in zebrafish as *Mtb* in humans, including the formation of granulomas (Swaim et al., 2006; Ramakrishnan, 2012), providing an interesting model system for studies on the pathogenesis of tuberculosis (Ramakrishnan, 2013; Cronan and Tobin, 2014; Torraca et al., 2014). We have utilized the previously described zebrafish tail fin infection model (Hosseini et al., 2014), which enables us to visualize the entire infection process from the first infected cells to the formation of early granuloma structures. For this purpose, time lapse confocal laser scanning microscopy (CLSM) in combination with advanced 3D block-face scanning electron microscopy (SBF-SEM) were used.

Results and discussion

Zebrafish larvae were infected with ~ 50 colony forming units (cfu) *M. marinum* (*Mm*) in the tail fin at 3 days post fertilization (dpf). We used larvae from a

transgenic line, *Tg(mpeg1:eGFP) X Tg(lys:DsRed)*, which displays green and red fluorescent of macrophages and neutrophils respectively (Ellett et al., 2011; Hall et al., 2007). Injection of *Mm* in the tail fin induces a localized infection, which attracts neutrophils and macrophages to the site of infection, and develops into a granuloma-like structure within 5 days post infection (dpi) (Fig. 1A) (Hosseini et al., 2014). Under basal conditions, the tail fin consists of two epithelial cell layers on both sides with mesenchyme cells in between and no leukocytes are normally found there (Kimmel et al., 1995). In order to provide a detailed description of the infection process and the host response, time-lapse imaging using confocal laser scanning microscopy (CLSM) was performed.

Bacterial burden and leukocyte recruitment

The bacterial burden and the number of macrophages and neutrophils recruited to the site of infection was quantified at 1, 6, 12 hours post infection (hpi) and at 1, 2, 3, 4 and 5 dpi (Fig. 1B-D). Representative images for these time points are shown in Fig. 1B. The bacterial burden does not change between 1 hpi and 1dpi, but increases significantly between 1 and 3 dpi after which it remains unchanged until 5 dpi (Fig. 1C). Upon infection, the number of recruited macrophages remains constant (at approximately 3) until 1 dpi, whereas the number of neutrophils decreases significantly from 4.2 (± 0.3) at 1 hpi to 1.1 (± 0.3) at 12 hpi (Fig. 1C). At this time point, the macrophages are the main type of leukocyte present at the site of infection and the majority of these macrophages (~72%) were infected with *Mm*. After this time point, both the number of macrophages and neutrophils increases dramatically and they remain constant after 4 dpi (Fig. 1C). Based on the bacterial burden at the site of infection, three different phases of the mycobacterial infection can be distinguished, the lag, exponential and stationary phase (Fig. 1E).

The lag phase of infection

To investigate the lag phase of infection, image sequences acquired using time-lapse microscopy were analyzed in detail focusing on leukocytes dynamics and cell death (Fig. 2, Suppl. Video 1). Figure 2A shows representative images of several time points during the lag phase of infection. These images show that during this lag phase the bacterial burden remains constant, the number of neutrophils decreases steadily and the number of macrophages remains constant but shows large fluctuations.

Using these image sequences the trajectories of the macrophages and neutrophils were analyzed until they had moved out of the image frame or had undergone cell death. The infected macrophages and neutrophils show short trajectories and the vast majority of these cells (~84%) remain local in the tail fin (Fig. 2B, 2C). A fraction of infected macrophages and neutrophils was observed to migrate away from the infection

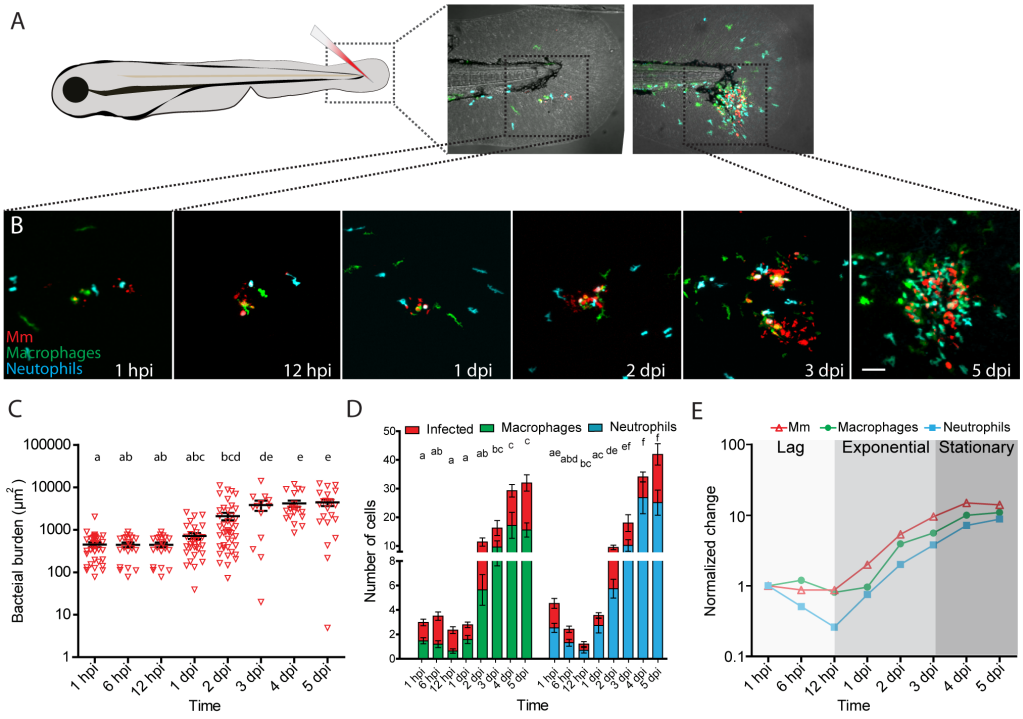

Fig. 1. Mycobacterium marinum infection in the zebrafish tail fin. A) Schematic image showing the location in the tail fin where Mm was injected into zebrafish larvae at 3 dpf. **B)** Representative CLSM images of the infection site in the tail fin at different time points. **C)** Quantification of the bacterial burden at different time points after Mm infection. **D)** Numbers of recruited macrophages (green) and neutrophils (blue) to the site of infection and their infected fractions (red) per larva. **E)** Normalized bacterial burden and numbers of recruited leukocytes (relative to 1 hpi). The analysis shows that based on the bacterial burden, the course of infection can be divided into three different phases: the lag, exponential and stationary phase. Error bars indicate standard error of the mean, n~20 larvae per timepoint. Means with the same letter do not differ significantly (Dunnett's post-test, $P<0.05$). Scale bar: 50 µm.

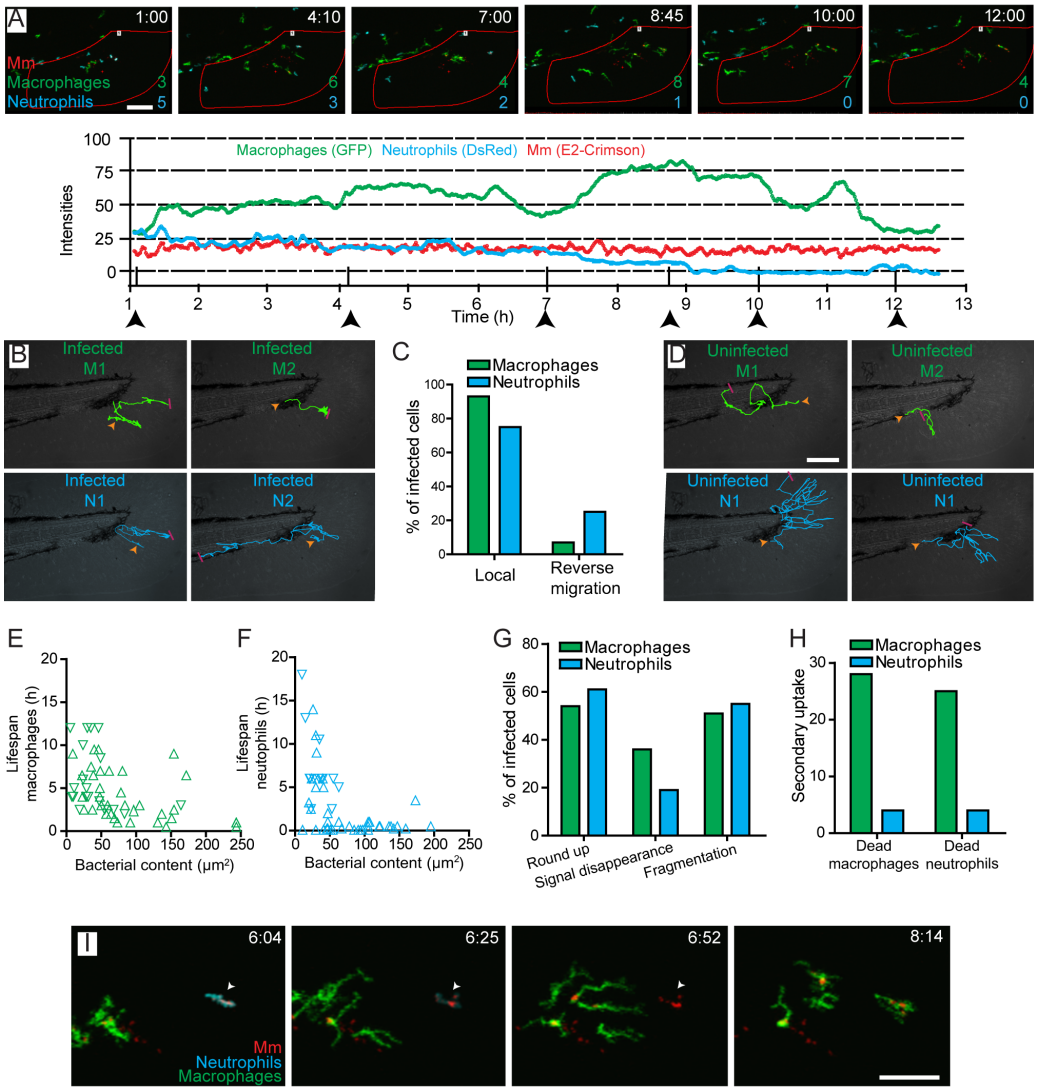

Fig. 2. Accumulation of Mm in macrophages occurs through cell death and secondary uptake by macrophages at the site of infection. A) Intensity profiles for macrophages (green), neutrophils (blue) and Mm (red) at the site of infection in a representative larva, showing dynamic recruitment and resolution of leukocytes. For time points indicated by the arrowheads corresponding images are shown, in which the numbers of leukocytes present within the region of interest (shown in red) are indicated . **B)** Representative trajectories of infected leukocytes. Macrophage 1 and neutrophil 1 show short local trajectories in the tail fin. Macrophage 2 was recruited to the site of infection and remains at the same position after phagocytosis of Mm. Neutrophil 2 showed reverse migration along the caudal vein. **C)** Percentages of leukocytes showing local and reverse migration. **D)** Representative trajectories of uninfected macrophages (green) and neutrophils (blue). The macrophages show short trajectories into and out of the tail fin, while the neutrophils show longer trajectories in the

tail fin before going out. **E and F)** Lifespan of infected leukocytes as a function of the infection size at the lag phase of infection. **G)** Percentages of infected leukocytes undergoing cell death showing different morphologies. **H)** Phagocytosis of bacterial content of leukocytes that have undergone cell death by macrophages and neutrophils. **I)** Representative frames from time-lapse imaging showing phagocytosis by a macrophage of bacterial content, which was initially sequestered inside a neutrophil. Scale bars: 50 μm.

site (Fig. 2C; infected N2). This reverse migration was observed for ~25% of all infected neutrophils compared to only ~7% of all infected macrophages (Fig 2C). Generally, these leukocytes migrate along the caudal vein (marked in Fig. 2C as infected N2) and were not observed to intravasate the caudal vein. Uninfected macrophages show short trajectories towards and away from the infection site, whereas neutrophils show longer trajectories covering a large area of the tail fin (Fig. 2D).

The role of macrophages in the dissemination of mycobacterial infections is well known, but the role of neutrophils is unclear (Davis and Ramakrishnan, 2009). A study in a murine infection model suggested that an attenuated *M. bovis* strain (BCG) after phagocytosis by neutrophil migrate via afferent lymphatics to lymphoid tissue and can spread bacterial infection (Abadie et al., 2005). Recent studies in a zebrafish larval infection model in which *E. coli* were injected subcutaneously, demonstrated phagocytosis of pathogens (including *Mm*) by neutrophils to be tissue-dependent,. (Colucci-Guyon et al., 2011; Belon et al., 2014). However, it was not observed upon injection of *Mm* into the bloodstream or the hindbrain of zebrafish larvae (Yang et al., 2012; Cui et al., 2011; Davis et al., 2002). Here we show that neutrophils can efficiently phagocytize mycobacteria at the initial infection site, and undergo reverse migration more frequent than macrophages. Due to their high mobility, neutrophils may disseminate bacteria further in the host than macrophages.

The lifespan of leukocytes is dependent on infection quantity

The image sequences were additionally used to determine the lifespan of neutrophils and macrophages after infection. Infected macrophages have an average lifespan of 4.8 (± 0.5) hours compared to 3.1 (± 0.6) for neutrophils. The bacterial content of these cells appears to correlate with their lifespan (Fig. 2E-F) showing that the higher the bacterial content the shorter their lifespan. For macrophages the lifespan shows a continuum, whereas for neutrophils we found a bimodal distribution. The majority of infected neutrophils have a very short lifespan (<1 h), and have a bacterial content larger than ~50 μm^2. Neutrophils with a smaller bacterial content have a longer lifespan.

Different morphologies of cell death

We show that infected leukocytes undergo massive cell death, which here is defined as a disappearance of the fluorescent signal. We could distinguish three different patterns for leukocytes undergo cell death, based on the fluorescent signal (Fig. 2G, Suppl. Fig. 1). The majority of leukocytes undergoing cell death display a round morphology before signal disappearance (54% macrophages, 61% neutrophils). The time between rounding up and signal disappearance varies from a few minutes to several hours. The second way of cell death we observed was fragmentation of the cell into several compartments, of which at least one contained bacteria. The fluorescent signal of these compartments disappeared at different rates, ranging from few minutes to hours. 51% of macrophages and 54% of neutrophils displayed this form of cell death. The third pattern of cell death was characterized by a rapid signal disappearance. In these leukocytes the fluorescent signal disappears within few minutes after ingestion of bacteria (suppl. Fig. 1B). 36% of macrophages and 19% of neutrophils underwent this form of cell death.

Phagocytosis of dead cells by macrophages

Regardless of the type of cell death of infected leukocytes, secondary uptake of the bacterial content was performed by the macrophages in most cases. This secondary uptake most likely includes phagocytosis of the remains of the dying or dead cells, which is called efferocytosis (Martin et al., 2014). The secondary uptake of bacterial content was observed to be phagocytized by macrophages in 87% of the cases, regardless of whether these bacteria had initially been sequestered by macrophages or neutrophils (Fig 2G). In the remaining ~13% of the cases this efferocytosis was carried out by neutrophils. In Figure 2I an example is shown of efferocytosis by a macrophage taking up an infected neutrophil which has undergone cell death (as shown by the rapid fluorescent signal disappearance).

Exponential phase of infection: 12 hours to 3 days post infection

At the beginning of this phase (12 hpi) the bacterial infection is mainly present in macrophages due to continuous neutrophilic cell death and efferocytosis during the lag phase. In order to study the progression of the infection from 12 hpi to 2 dpi, we analyzed time-lapse recordings for this period. Two events are characteristic for the infection process after 12 hpi: macrophage burst and extrusion of bacteria (Fig. 3).

Macrophage burst events

In our study, macrophage burst events were defined as large compacted bacterial aggregates inside macrophages that spread to the surrounding tissue, probably due to cell death-induced rupture of the membranes surrounding the bacteria (Repasy

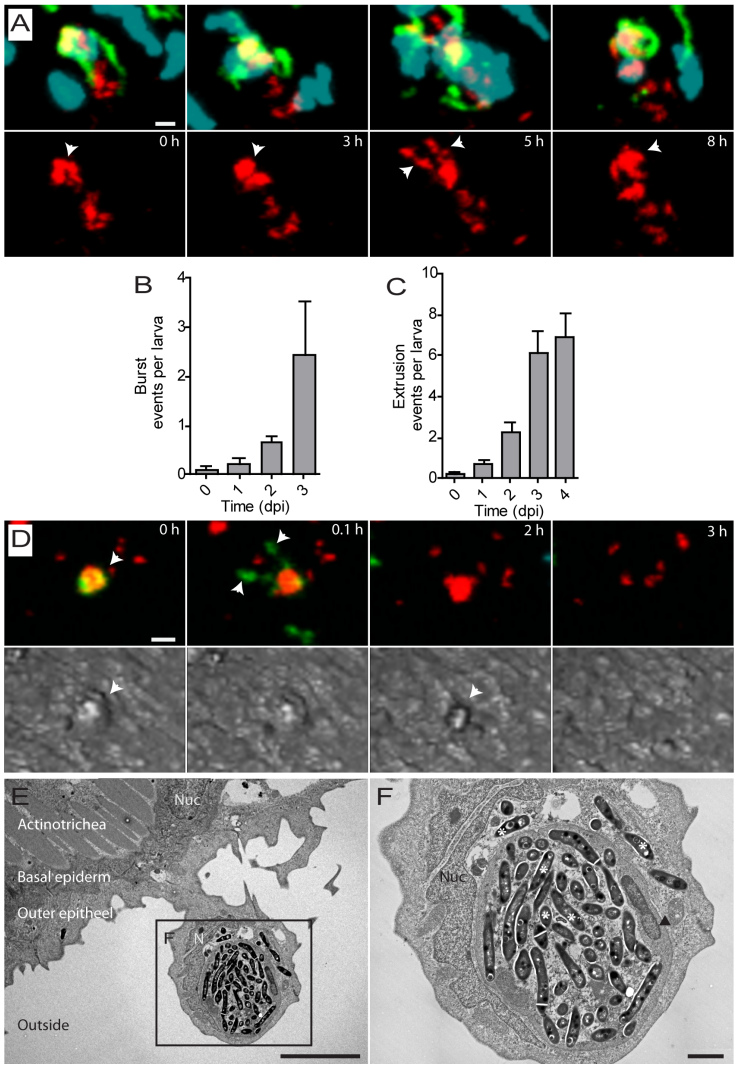

Fig. 3. Macrophages containing aggregates of Mm undergo burst or extrusion. A) Representative images from live cell imaging of a large aggregate of Mm (arrowhead) inside a macrophage (arrow) undergoing cell death at t=3h. Spreading of Mm was observed at t=5h. The aggregate was compacted again by newly recruited leukocytes at t=8h (see also Video 2.mov). **B)** Number of burst events observed at different time points after Mm infection in the tail fin. **C)** Number of extrusion events observed at different time points after Mm infection in the tail fin. **D)** Representative images from live cell imaging showing an extrusion event of accumulated Mm in a macrophage. First, the macrophage undergoes cell death and subsequently after 3 hours the bacterial content is extruded. **E)** TEM image of an extruding epithelial cell from the tail fin surrounding a dead cell containing a large aggregate of Mm. The two epithelial layers and actinotrichia collagens are indicated. **F)** Higher magnification of the region indicated in E, showing compact aggregates of Mm (asterisks) in the dead cell with a condensed nucleus (arrow head). Error bas indicate SEM. Scale bars in A, C and E: 10 µm; in F: 2 µm.

et al., 2013). Subsequently, the spread bacteria are taken up by neutrophils and macrophages. An example of such a burst event imaged using time-lapse CLSM is shown in Fig. 3A and Video 2. The number of burst events increases dramatically between 1 and 3 dpi, from 0.1 (±0.08) to 2.4 (±1.1) burst events per larva. This is probably due to the increased bacterial burden per cell.

Extrusion of *Mm* aggregates

Interestingly, large aggregates of bacteria were also observed to be extruded out of the tail fin. The frequency of these extrusion events had significantly increased between 1 and 3 dpi, from 0.8 (±0.1) to 6.9 (±1.1) extrusion events per larva (Fig. 3C). An example of an extrusion event imaged using time-lapse CLSM is shown in Fig. 3D and Video 3. As in most cases, in this example the bacterial content was initially present in a macrophage, and was extruded 2 to 3 hours after disappearance of the fluorescent signal of the macrophage. These extrusion events were not exclusively observed upon cell death of macrophages, but occur occasionally after neutrophil cell death as well. The extruded bacterial aggregate displays itself first as a protuberance on the outer epithelial layer of the tail fin, which could be observed using brightfield/DIC microscopy (Fig. 3D). The ultrastructure of such a protuberance was imaged using TEM (Fig. 3E-F). These images show a bacterial aggregate shortly before an extrusion event. A cell of the outer epithelial layer contains a dead cell with a large bacterial aggregate, and is in the process of being extruded from the epithelial layer.

Extrusion of dead or infected epithelial cells is important for the preservation of the epithelial barrier (Gu and Rosenblatt, 2012; Eisenhoffer et al., 2012). Apical extrusion of Salmonella-infected epithelial cells into the lumen has been observed in the gall bladder of infected mice (Knodler et al., 2010). To our knowledge this process has not been shown for mycobacterium infection. The role of extrusion by lung epithelium is still unclear. In the case of *Mtb* infection that primarily affects the lungs in humans, this process might represent an important mechanism in the clearance of *Mtb*. Alternatively, mycobacteria inside extruded cells could be used by the pathogen as a strategy for avoiding the pro-inflammatory response and dissemination from human to human.

Stationary phase of infection: 3 days post infection

The stationary phase of larval infection is characterized by granuloma-like structures containing a large number of macrophages and neutrophils at the site of infection. In addition, at this phase we observe secondary granuloma-like structures (suppl. Fig. 2), which are most often observed near the caudal vein. Additionally, at this phase extrusion occurs at a large scale and the bacterial content of several cells were observed to be simultaneously extruded.

Ultrastructure of infected macrophages and neutrophils

In order to get a deeper understanding of cellular processes ongoing in the infected leukocytes observed during time-lapses, infected larvae were analyzed using EM. We used 3D block-face SEM to obtain a 3D EM image of the region of the infected tail fin at 3 dpi (Video 4). In this technique, EM images are acquired from the surface of the tissue sample. Subsequently, a 100 nm layer is removed and a new image of the surface is acquired (Denk and Horstmann, 2004; Peddie and Collinson, 2014). To correlate these 3D EM images with the images obtained by CLSM, the bacteria observed in the EM images were aligned with the fluorescent signal of *Mm* acquired by CLSM (Suppl. Fig.2). By aligning the images acquired by the two techniques, the fluorescently labeled macrophages and neutrophils were identified in EM images (Fig. 4A-B). Using this approach the EM images of the infected macrophages and neutrophils could not only be correlated with the CLSM images, but could also be linked to the dynamic behavior of these cells in the previous hours (Video 5).

The images of two infected macrophages and two infected neutrophils were correlated (indicated in Fig. 4A-B). The EM image of the first macrophage shows clear chromatin condensation in the nucleus indicating that this cell is undergoing apoptosis (Fig. 4D). The confocal images show that this cell has phagocytized a large aggregate of bacteria ~30 minutes earlier (Fig.4C). Although mycobacteria are notorious for their ability to block apoptosis (Lee et al., 2006; Repasy et al., 2013), here we show that macrophages with a large bacterial content, most likely acquired by efferocytosis, may undergo apoptosis (Fig. 4D). In addition, infected macrophages showing clear fragmentation, another hallmark of apoptotic cell death, was observed using light microscopy (Fig. 2G, Suppl. Fig. 1D). The second imaged macrophage contains a single compartment containing a bacterial aggregate and remains of dead cells (Fig 4D). The confocal images show that this macrophage had phagocytized the aggregate ~1.5 hour earlier and no sign of cell death is shown yet in the EM image (Fig. 4C).

The first imaged neutrophil displays a necrotic morphology, characterized by a round nucleus and an irregularly shaped plasma membrane and no apoptotic features (Fink and Cookson, 2005). In the confocal images this neutrophil showed a compacted bacterial content at the start of the time-lapse and a disappearance of the fluorescent signal (within 1 min) approximately 30 minutes before fixation (Fig 4C). Based on light microscopy observations, the rapid signal disappearance of uninfected neutrophils was previously suggested to be apoptosis (Loynes et al., 2010). However, based on these correlated light and EM images, we suggest that the type of cell death characterized by a rapid disappearance of the fluorescent signal (<1 minute) is a form of necrotic cell death. By fusion of lysosomal compartments with the cytoplasm (Artal-Sanz et al., 2006) and probably the release of abundant peroxides present in neutrophils, necrotic cells may lose their fluorescence due to a rapid denaturation

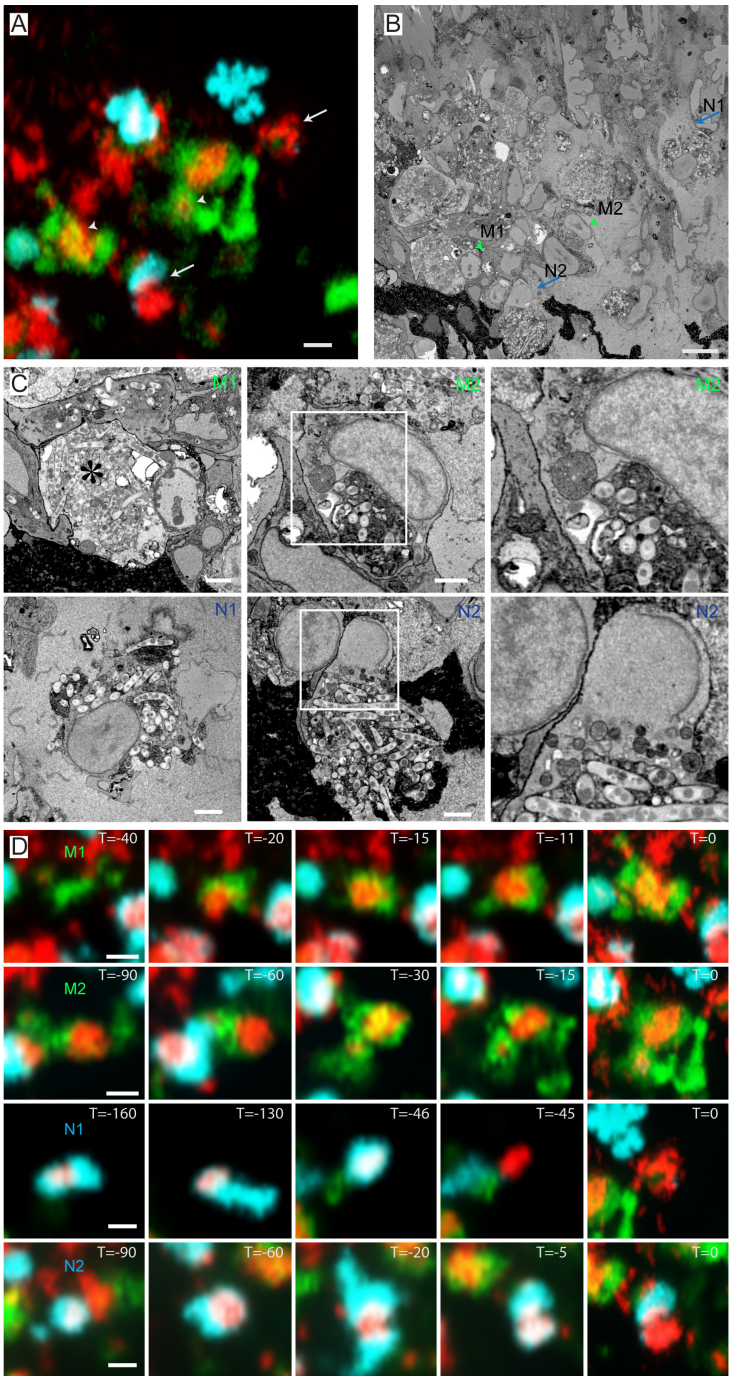

Fig. 4. Ultrastructure of correlated macrophages and neutrophils in 3D block-face SEM images. A) High resolution CLSM image of an infected tail fin after live cell imaging and fixation. **B)** BF-SEM image of the same region in (A) showing correlated macrophages (arrowheads) and neutrophils (arrows). **C)** Higher magnification BF-SEM images of the two macrophages and two neutrophils indicated in A and B. **D)** Frames from time-lapse imaging showing the macrophages and neutrophils in (C) at previous time points. The early stage apoptotic macrophage (M1) contains a high Mm content indicated by asterisk in (C). This macrophage phagocytized the bacterial content ~30 minutes before fixation. Macrophage (M2) contains a large aggregate of Mm which was phagocytized Mm ~1,5 hours before fixation. Neutrophil (N1) showed rapid signal disappearance ~45 minutes before the fixation (D). Neutrophil (N2) was recruited to the bacterial aggregate ~ 30 minutes before fixation (D). Scale bars: A-C, 10 µm; D, 2 µm.

of the fluorescent proteins. The second imaged neutrophil has not entirely engulfed the bacterial aggregate. Instead, this neutrophil seems to be in a process called netosis (Francis et al., 2014). It shows a nuclear membrane that is not intact and granules at the plasma membrane fusing with the extracellular space, in which a large aggregate of bacteria is located (Fig 4D and Video 6). In confocal images this cell was observed to be interacting with a large aggregate of *Mm* in the preceding 30 min, which was previously contained by another neutrophil (Fig 4C). Netosis is often associated with necrotic infected neutrophils (Francis et al., 2014). Neutrophils are able to sense microbe size and selectively release extracellular traps in response to large pathogens, such as *Candida albicans* hyphae and extracellular aggregates of *Mycobacterium bovis* (Branzk et al., 2014).

In the BF-SEM images we also observed *Mm* infected epithelial cells in the process of undergoing extrusion (Suppl. Fig.2D). These cells did not show a fluorescent signal associated with macrophages or neutrophils. Using 3D information provided by this method, we could observe that the bacterial aggregate was entirely contained within an epithelial cell. The presence of a bacterial aggregate inside an epithelial cell indicates bacterial uptake at the basal side of the cell (probably by efferocytosis), which subsequently undergoes extrusion at the apical side.

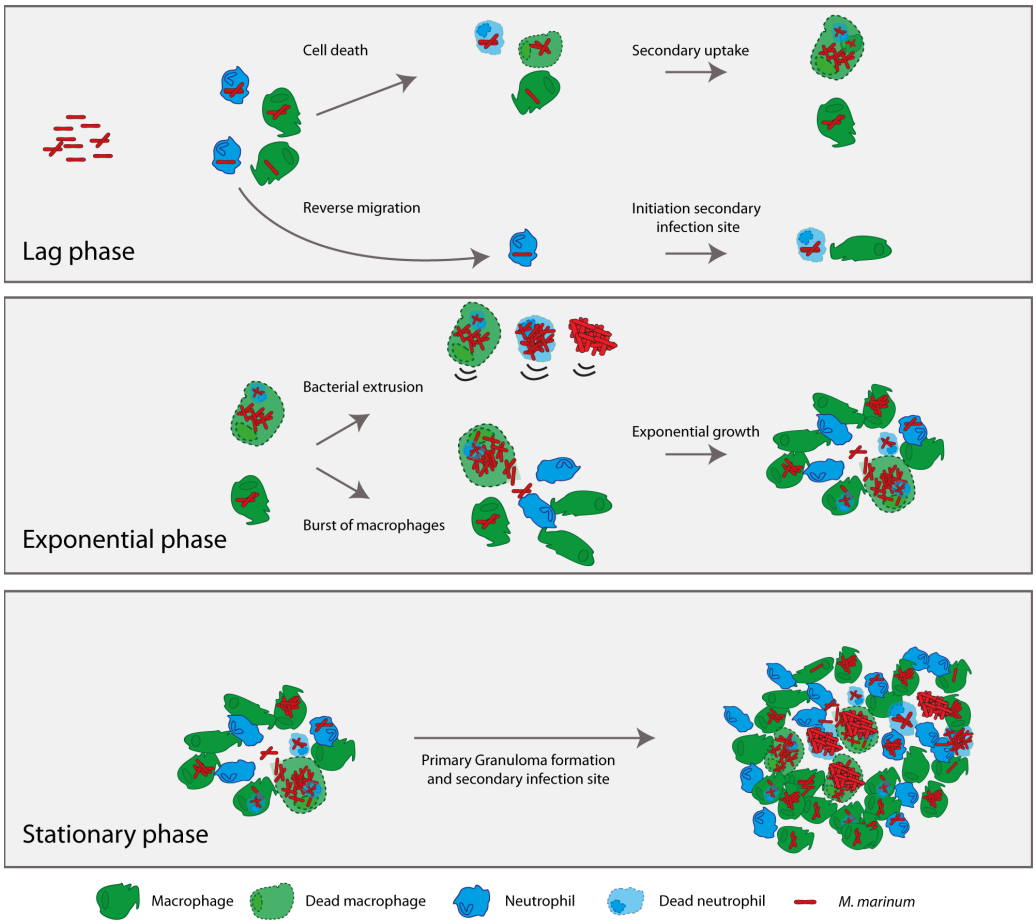

Fig. 5. Overview of Mm infection in the tail fin of zebrafish larvae. This overview summarizes the processes taking place during the course of infection.

Conclusions

In the present study we show the specific key functions of macrophages and neutrophils during the dynamic infection process of *Mm* in zebrafish larvae. In Figure 5 a schematic overview is shown of the cellular processes during the different phases of early granuloma development observed in this study.

Following the dynamics of the leukocytes during the course of infection, we found that many macrophages and neutrophils undergo cell death during the process of infection. As a result the number of leukocytes involved in the infection process will be underestimated when single time points are investigated. We show that the neutrophils are efficient in phagocytosis of *Mm* and contribute largely to

the dissemination of the bacteria. The macrophages appear to play a major role in efferocytosis of dead infected macrophages and neutrophils. Continuous efferocytosis by macrophages results in high bacterial contents in these cells, resulting in burst of macrophages when they are unable to retain the pathogen. Finally, epithelially mediated extrusion of the bacterial content after efferocytosis of infected leukocytes was observed to contribute to bacterial clearance.

Materials and Methods

Zebrafish strains and maintenance

Zebrafish were handled in compliance with the local animal welfare regulations and maintained according to standard protocols (www.zfin.org). The ABTL wild type zebrafish strain and the transgenic lines, *Tg(mpeg1:eGFP),* and *Tg(lys:DsRed),* strains were used for this study. All fish were raised and grown at 28.5 °C on a 14 h light : 10 h dark cycle. Embryos were obtained from natural spawning at the beginning of the light period and kept in egg water (60 µg/ml Instant Ocean sea salts).

Zebrafish tail fin infection

The *M. marinum* M strain fluorescently labeled with E2-crimson was used and prepared at ~500 colony-forming units per 1 nl as previously described (Benard et al., 2012). Borosilicate glass micro capillaries (Harvard Apparatus, 300038) were used with a micropipette puller device (Sutter Instruments Inc.) for preparing microinjection needles. Zebrafish larvae were injected in the tail fin at 3 dpf using the Eppendorf microinjection system with a fine (~5 to 10 micron) needle tip broken off with tweezers and mounted at a 30-degree angle. Larvae were anesthetized in egg water with 200 µg/mL 3-aminobenzoic acid (Tricaine; Sigma-Aldrich, E10521) and injected between the two epidermal layers at the ventral part of the tail fin (Fig. 1).

Confocal laser scanning microscopy

Larvae were anesthetized with 200 µg/ml tricane and mounted in 0.7% low melting agarose (Sigma-Aldrich, A9414) and imaged with the Nikon A1 confocal laser scanning microscope (Tokyo, Japan) using the 488, 561 and 641 laser lines with 20X (NA 0.75). Images were analyzed using NIS-Elements analysis software. The bacterial burden was analyzed on the max-projection images (12 bit), binary areas were created based on the *M. marinum* fluorescent signal using a threshold

above 900 for the larvae at 0 dpi to 2 dpi and threshold above 1700 for larvae from 3 dpi to 5 dpi. The number of macrophages and neutrophils and all the events were counted manually. The tracks were generated using Nis elements 4 (Nikon software) and manually corrected miss matched tracks. The macrophage and neutrophil interactions during infection 225 larvae were imaged at ~60 seconds per frame for 18 hours at 28.5 degrees. For the lag fase 33 larvae were analyzed (n= 70 macrophages and 70 neutrophils) between 6 and 18 hours, larvae moved out of view in less than 6 hours were removed from analyses. For the exponential phase 60 larvae and for the stationary phase 40 larvae were analyzed. The clearly observable macrophage burst events were counted manually and the bacterial extrusion events were scored manually to a maximum of 10 events per larva based on bacterial content released from the tissue.

Transmission electron microscopy

Before being used for electron microscopy the zebrafish larvae were anesthetized with 200 µg/ml tricaine and fixated in 2% glutaraldehyde and 2% paraformaldehyde in sodium cacodylate buffer (pH 7.2) for 3 h at room temperature followed by fixation for 16 h at 4 °C. Post fixation was performed in 1% osmium tetroxide in sodium cacodylate buffer for 1 h at room temperature. After dehydration through a graded series of ethanol all specimens were kept in epoxy resin (Agar Scientific, AGR1043) for 16 h before embedding. Ultrathin sections were collected on Formvar coated one hole copper grids (Agar Scientific, AGS162) stained with 2% uranyl acetate in 50% ethanol and lead citrate for 10 min each. Electron microscopy images were obtained with a JEOL JEM-1010 transmission electron microscope (Tokyo, Japan) equipped with an Olympus Megaview camera (Tokyo, Japan).

Block-Face scanning electron microscopy

The larvae were prepared using a protocol modified from (Deerinck et al., 2010). Before being used for block-face scanning electron microscopy the zebrafish larvae were anesthetized with 200 µg/ml tricaine, imaged alive by CLSM and afterwards immediately fixated in 0.5% glutaraldehyde and 2% paraformaldehyde in PHEM buffer (pH 6.9) for 2 h at room temperature followed by fixation in 2% glutaraldehyde and 2% paraformaldehyde in sodium cacodylate buffer (pH 7.2) for 16 h at 4 °C. Postfixation was performed in 1:1 4% Osmium tertroxide : 3% K Ferrocyanide in 0,3 M Na cacodylate buffer (pH 7,2), 20 min 1 % ThioCarboHydrazide (TCH), 30 min 2% Osmium tertroxide, 1 hr 1% Uranyl Acetate and 30 min Waltons Lead aspartate at 60°C. After dehydration through a graded series of ethanol all specimens were kept in epoxy resin (Agar Scientific, AGR1043) for 16 h before embedding. Blocks were trimmed and glued on a cryopin and examined in a Quanta FEG 250 with a Gatan 3View Ultramicrotome module using the BSE mode to perform 3D block-face

images by cutting 150 nm sections. The data was segmented and aligned with CLSM images using Amira 3.5 (FEI, USA) software.

Statistical analysis

All data were analyzed (Prism version 5.0, GraphPad Software) using one-way analysis of variance (ANOVA) with Dunnett's post-test for multiple groups. Error bars represent mean ± SEM, statistical significance was assumed at *p*-value below 0.05.

Acknowledgements

We thank Tobias Starborg (University of Manchester) for technical assistant and Bram Koster (LUMC) for helpful discussion. Infectious disease research in our laboratory is supported by the European Commission 7th framework project ZF-HEALTH (HEALTH-F4-2010-242048) and the Cyttron II Program (LSH framework: FES0908).

References

Abadie, V., E. Badell, P. Douillard, D. Ensergueix, P.J.M. Leenen, M. Tanguy, L. Fiette, S. Saeland, B. Gicquel, and N. Winter. 2005. Neutrophils rapidly migrate via lymphatics after Mycobacterium bovis BCG intradermal vaccination and shuttle live bacilli to the draining lymph nodes. *Blood*. 106:1843–1850. doi:10.1182/blood-2005-03-1281.

Artal-Sanz, M., C. Samara, P. Syntichaki, and N. Tavernarakis. 2006. Lysosomal biogenesis and function is critical for necrotic cell death in Caenorhabditis elegans. *The Journal of Cell Biology*. 173:231–239. doi:10.1083/jcb.200511103.

Benard, E.L., A.M. van der Sar, F. Ellett, G.J. Lieschke, H.P. Spaink, and A.H. Meijer. 2012. Infection of zebrafish embryos with intracellular bacterial pathogens. *J Vis Exp*. doi:10.3791/3781.

Berry, M.P.R., C.M. Graham, F.W. McNab, Z. Xu, S.A.A. Bloch, T. Oni, K.A. Wilkinson, R. Banchereau, J. Skinner, R.J. Wilkinson, C. Quinn, D. Blankenship, R. Dhawan, J.J. Cush, A. Mejias, O. Ramilo, O.M. Kon, V. Pascual, J. Banchereau, D. Chaussabel, and A. O'Garra. 2010. An interferon-inducible neutrophil-driven blood transcriptional signature in human tuberculosis. *Nature*. 466:973–977. doi:10.1038/nature09247.

Branzk, N., A. Lubojemska, S.E. Hardison, Q. Wang, M.G. Gutierrez, G.D. Brown, and V. Papayannopoulos. 2014. Neutrophils sense microbe size and selectively release neutrophil extracellular traps in response to large pathogens. *Nat. Immunol.* 15:1017–1025. doi:10.1038/ni.2987.

Colucci-Guyon, E., J.-Y. Tinevez, S.A. Renshaw, and P. Herbomel. 2011. Strategies of professional phagocytes in vivo: unlike macrophages, neutrophils engulf only surface-associated microbes. *Journal of Cell Science*. 124:3053–3059. doi:10.1242/jcs.082792.

Cronan, M.R., and D.M. Tobin. 2014. Fit for consumption: zebrafish as a model for tuberculosis. *Dis Model Mech*. 7:777–784. doi:10.1242/dmm.016089.

Cui, C., E.L. Benard, Z. Kanwal, O.W. Stockhammer, M. van der Vaart, A. Zakrzewska, H.P. Spaink, and A.H. Meijer. 2011. Infectious disease modeling and innate immune function in zebrafish embryos. *Methods Cell Biol.* 105:273–308. doi:10.1016/B978-0-12-381320-6.00012-6.

Davis, J.M., H. Clay, J.L. Lewis, N. Ghori, P. Herbomel, and L. Ramakrishnan. 2002. Real-time visualization of mycobacterium-macrophage interactions leading to initiation of granuloma formation in zebrafish embryos. *Immunity*. 17:693–702.

Deerinck, T.J., E.A. Bushong, A. Thor, and M.H. Ellisman. 2010. NCMIR methods for 3D EM: a new protocol for preparation of biological specimens for serial block face scanning electron microscopy. 1–3.

Denk, W., and H. Horstmann. 2004. Serial block-face scanning electron microscopy to reconstruct three-dimensional tissue nanostructure. *Plos Biol*. 2:e329. doi:10.1371/journal.pbio.0020329.

Eisenhoffer, G.T., P.D. Loftus, M. Yoshigi, H. Otsuna, C.-B. Chien, P.A. Morcos, and J. Rosenblatt. 2012. Crowding induces live cell extrusion to maintain homeostatic cell numbers in epithelia. *Nature*. 484:546–549. doi:10.1038/nature10999.

Elks, P.M., S. Brizee, M. van der Vaart, S.R. Walmsley, F.J. van Eeden, S.A. Renshaw, and A.H. Meijer. 2013. Hypoxia inducible factor signaling modulates susceptibility to mycobacterial infection via a nitric oxide dependent mechanism. *PLoS Pathog*. 9:e1003789. doi:10.1371/journal.ppat.1003789.

Ellett, F., L. Pase, J.W. Hayman, A. Andrianopoulos, and G.J. Lieschke. 2011. mpeg1 promoter transgenes direct macrophage-lineage expression in zebrafish. *Blood*. 117:e49–e56. doi:10.1182/blood-2010-10-314120.

Eum, S.-Y., J.-H. Kong, M.-S. Hong, Y.-J. Lee, J.-H. Kim, S.-H. Hwang, S.-N. Cho, L.E. Via, and C.E. Barry. 2010. Neutrophils are the predominant infected phagocytic cells in the airways of patients with active pulmonary TB. *Chest*. 137:122–128. doi:10.1378/chest.09-0903.

Fink, S.L., and B.T. Cookson. 2005. Apoptosis, Pyroptosis, and Necrosis: Mechanistic Description of Dead and Dying Eukaryotic Cells. *Infect. Immun.* 73:1907–1916. doi:10.1161/01.CIR.98.14.1422.

Francis, R.J., R.E. Butler, and G.R. Stewart. 2014. Mycobacterium tuberculosis ESAT-6 is a leukocidin causing Ca2+ influx, necrosis and neutrophil extracellular trap formation. *Cell Death Dis*. 5:e1474. doi:10.1038/cddis.2014.394.

Gu, Y., and J. Rosenblatt. 2012. New emerging roles for epithelial cell extrusion. *Current Opinion in Cell Biology*. 24:865–870. doi:10.1016/j.ceb.2012.09.003.

Hall, C., M.V. Flores, T. Storm, K. Crosier, and P. Crosier. 2007. The zebrafish lysozyme C promoter drives myeloid-specific expression in transgenic fish. *BMC Dev. Biol.* 7:42. doi:10.1186/1471-213X-7-42.

Hosseini, R., G.E. Lamers, Z. Hodzic, A.H. Meijer, M.J. Schaaf, and H.P. Spaink. 2014. Correlative light and electron microscopy imaging of autophagy in a zebrafish infection model. *autophagy*. 10:1844–1857. doi:10.4161/auto.29992.

Kimmel, C.B., W.W. Ballard, S.R. Kimmel, B. Ullmann, and T.F. Schilling. 1995. Stages of embryonic development of the zebrafish. *Dev. Dyn.* 203:253–310. doi:10.1002/aja.1002030302.

Knodler, L.A., B.A. Vallance, J. Celli, S. Winfree, B. Hansen, M. Montero, and O. Steele-Mortimer. 2010. Dissemination of invasive Salmonella via bacterial-induced extrusion of mucosal epithelia. *Proc. Natl. Acad. Sci. U.S.A.* 107:17733–17738. doi:10.1073/pnas.1006098107.

Lee, J., H.G. Remold, M.H. Ieong, and H. Kornfeld. 2006. Macrophage apoptosis in response to high intracellular burden of Mycobacterium tuberculosis is mediated by a novel caspase-independent pathway. *J Immunol*. 176:4267–4274.

Martin, C.J., K.N. Peters, and S.M. Behar. 2014. Macrophages clean up: efferocytosis and microbial control. *Curr. Opin. Microbiol.* 17:17–23. doi:10.1016/j.mib.2013.10.007.

Nouailles, G., A. Dorhoi, M. Koch, J. Zerrahn, J. Weiner, K.C. Faé, F. Arrey, S. Kuhlmann, S. Bandermann, D. Loewe, H.-J. Mollenkopf, A. Vogelzang, C. Meyer-Schwesinger, H.-W. Mittrücker, G. McEwen, and S.H.E. Kaufmann. 2014. CXCL5-secreting pulmonary epithelial cells drive destructive neutrophilic inflammation in tuberculosis. *J. Clin. Invest.* 124:1268–1282. doi:10.1172/JCI72030.

Peddie, C.J., and L.M. Collinson. 2014. Exploring the third dimension: volume electron microscopy comes of age. *Micron*. 61:9–19. doi:10.1016/j.micron.2014.01.009.

Ramakrishnan, L. 2012. Revisiting the role of the granuloma in tuberculosis. *Nat Rev Immunol*.

Ramakrishnan, L. 2013. An interview with Lalita Ramakrishnan. *Trends Pharmacol. Sci.* 34:197. doi:10.1016/j.tips.2013.02.005.

Renshaw, S.A., C.A. Loynes, D.M.I. Trushell, S. Elworthy, P.W. Ingham, and M.K.B. Whyte. 2006. A transgenic zebrafish model of neutrophilic inflammation. *Blood*. 108:3976–3978. doi:10.1182/blood-2006-05-024075.

Repasy, T., J. Lee, S. Marino, N. Martinez, D.E. Kirschner, G. Hendricks, S. Baker, A.A. Wilson, D.N. Kotton, and H. Kornfeld. 2013. Intracellular bacillary burden reflects a burst size for Mycobacterium tuberculosis in vivo. *PLoS Pathog*. 9:e1003190. doi:10.1371/journal.ppat.1003190.

Silva, M.T., M.N. Silva, and R. Appelberg. 1989. Neutrophil-macrophage cooperation in the host defence against mycobacterial infections. *Microb. Pathog.* 6:369–380.

Srivastava, S., J.D. Ernst, and L. Desvignes. 2014. Beyond macrophages: the diversity of mononuclear cells in tuberculosis. *Immunological Reviews*. 262:179–192. doi:10.1111/imr.12217.

Swaim, L.E., L.E. Connolly, H.E. Volkman, O. Humbert, D.E. Born, and L. Ramakrishnan. 2006. Mycobacterium marinum infection of adult zebrafish causes caseating granulomatous tuberculosis and is moderated by adaptive immunity. *Infect. Immun.* 74:6108–6117. doi:10.1128/IAI.00887-06.

Torraca, V., S. Masud, H.P. Spaink, and A.H. Meijer. 2014. Macrophage-pathogen interactions in infectious diseases: new therapeutic insights from the zebrafish host model. *Dis Model Mech*. 7:785–797. doi:10.1242/dmm.015594.

Volkman, H.E., H. Clay, D. Beery, J.C.W. Chang, D.R. Sherman, and L. Ramakrishnan. 2004. Tuberculous granuloma formation is enhanced by a mycobacterium virulence determinant. *Plos Biol*. 2:e367. doi:10.1371/journal.pbio.0020367.

Yang, C.-S., D.-M. Shin, H.-M. Lee, J.W. Son, S.J. Lee, S. Akira, M.-A. Gougerot-Pocidalo, J. El-Benna, H. Ichijo, and E.-K. Jo. 2008. ASK1-p38 MAPK-p47phox activation is essential for inflammatory responses during tuberculosis via TLR2-ROS signalling. *Cellular Microbiology*. 10:741–754. doi:10.1111/j.1462-5822.2007.01081.x.

Yang, C.-T., C.J. Cambier, J.M. Davis, C.J. Hall, P.S. Crosier, and L. Ramakrishnan. 2012. Neutrophils exert protection in the early tuberculous granuloma by oxidative killing of mycobacteria phagocytosed from infected macrophages. *Cell Host and Microbe*. 12:301–312. doi:10.1016/j.chom.2012.07.009.

Supplementary data

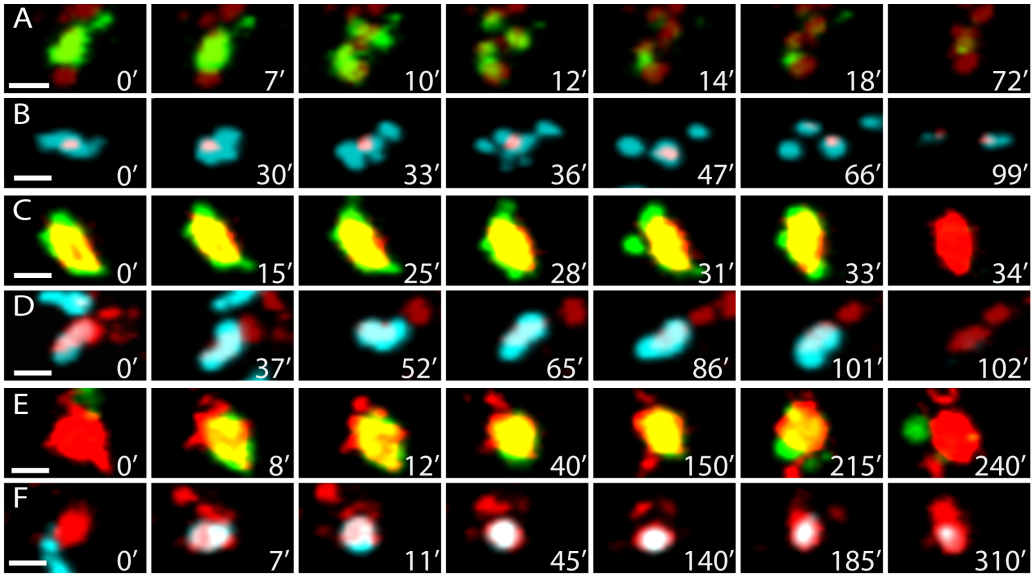

Suppl. Fig. 1. Different cell death morphologies of Mm infected macrophages and neutrophils. A and B) Selected frames taken from the image sequences of a macrophage **(A)** and a neutrophil **(B)** showing fragmentation of the cell in several compartment. **C and D)** Selected frames taken from the image sequences of a macrophage **(C)** and a neutrophil **(D)** showing rapid disappearance of the fluorescent signal. **E and F)** Selected frames taken from the image sequences of a macrophage (**E)** and a neutrophil **(F)** showing rounding up of the cell. Scale bars: 10 μm.

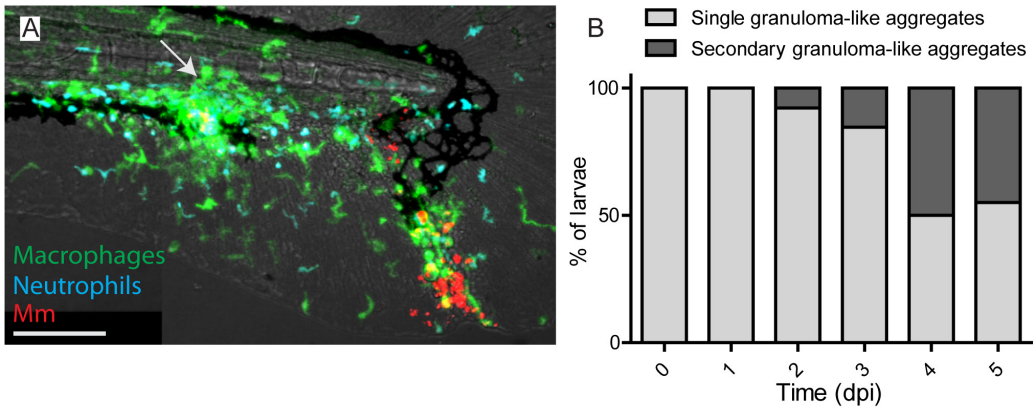

Suppl. Fig. 2. Secondary granulomas at stationary phase of infection. A) Representative image of an infected tail fin showing a secondary granuloma like aggregate (arrow) near the caudal vein. **B)** Percentage of larvae showing formation of a secondary granuloma like aggregate at different stages of infection. Scale bar: 100 μm.

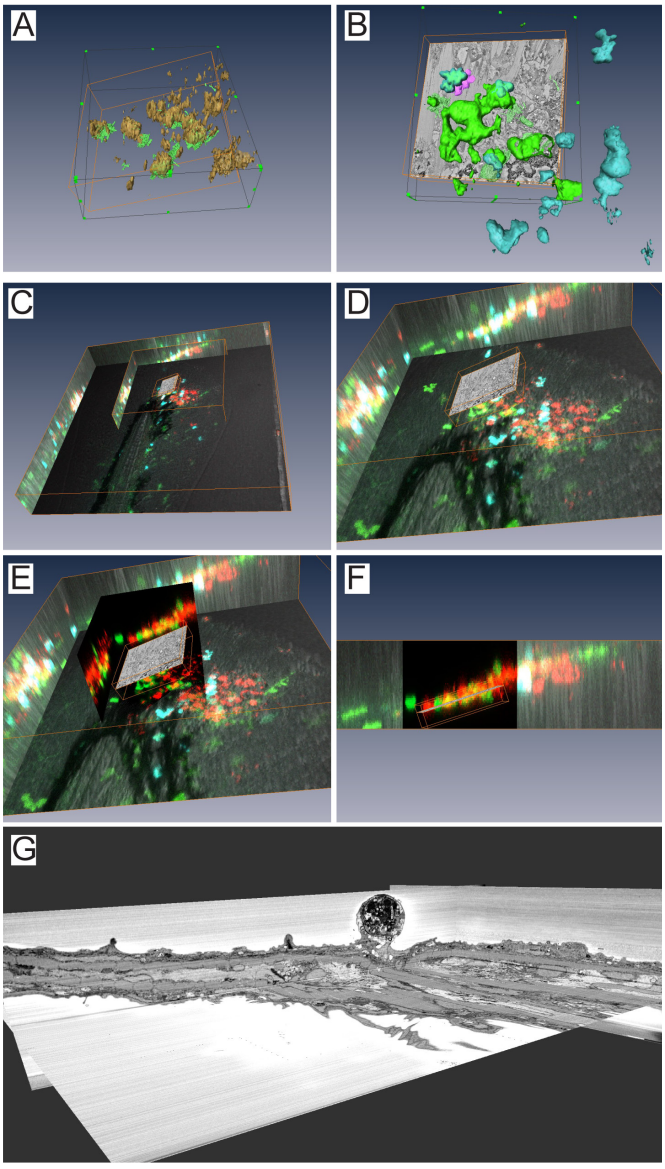

Suppl. Fig. 3. Correlation of the CLSM and 3D block-face SEM images. A) Alignment of Mm volumes imaged by CLSM and BF-SEM. The Mm in BF-SEM images were segmented and the 3D rendered surface of this segmentation is shown in green. The 3D rendered surface of the fluorescent signal obtained using CLSM is shown in yellow. B) Surface rendering of the macrophage (green) and neutrophil (blue) fluorescent signal was used after alignment to localize the macrophages and neutrophils in BF-SEM images. **C-F)** Aligned BF-SEM images projected in the 3D CLSM images shown from different angles. **G)** Orthogonal slices of BF-SEM images showing extrusion of a Mm aggregate from the outer epithelial layer.

Suppl. Fig. 1. Different cell death morphologies of *Mm* infected macrophages and neutrophils. A and B) Selected frames taken from the image sequences of a macrophage **(A)** and a neutrophil **(B)** showing fragmentation of the cell in several compartment. **C and D)** Selected frames taken from the image sequences of a macrophage **(C)** and a neutrophil **(D)** showing rapid disappearance of the fluorescent signal. **E and F)** Selected frames taken from the image sequences of a macrophage (**E)** and a neutrophil **(F)** showing rounding up of the cell. Scale bars: 10 μm.

Suppl. Fig. 2. Secondary granulomas at stationary phase of infection. A) Representative image of an infected tail fin showing a secondary granuloma like aggregate (arrow) near the caudal vein. **B)** Percentage of larvae showing formation of a secondary granuloma like aggregate at different stages of infection. Scale bar: 100 μm.

Suppl. Fig. 3. Correlation of the CLSM and 3D block-face SEM images. A) Alignment of *Mm* volumes imaged by CLSM and BF-SEM. The *Mm* in BF-SEM images were segmented and the 3D rendered surface of this segmentation is shown in green. The 3D rendered surface of the fluorescent signal obtained using CLSM is shown in yellow. B) Surface rendering of the macrophage (green) and neutrophil (blue) fluorescent signal was used after alignment to localize the macrophages and neutrophils in BF-SEM images. **C-F)** Aligned BF-SEM images projected in the 3D CLSM images shown from different angles. **G)** Orthogonal slices of BF-SEM images showing extrusion of a *Mm* aggregate from the outer epithelial layer.

Video 1. Macrophage and neutrophil behavior at the lag phase of *M. marinum* infection. Double transgenic *Tg(mpeg1:EGFP)* and *Tg(lys:DsRed)* larvae infected with *M. marinum* (red) were imaged alive every ~60 sec from 1 hpi to 12 hpi by CLSM (Nikon A1). In the top panel the dynamics of GFP-positive (green) macrophages and DsRed-positive (blue) neutrophils are shown, whereas in the bottom panels the trajectories for macrophages (left) and neutrophils (right) are indicated. The magenta and red lines represent infected macrophages and neutrophils, whereas the yellow and blue lines represent uninfected leukocytes. The infected cells remain in the tail fin, except for one of the neutrophils (red line), which undergoes reverse migration along the caudal vein. The uninfected macrophages show short trajectories in the tail fin and the neutrophils show longer tracks, of which one neutrophil (blue line) seems to be scanning a large area of the tail fin. The maximum intensity projection from 11 CLSM images (step size in z-direction, 5.56 μm) is shown at 10 frames per second. Scale bar: 100 μm.

Video 2. Macrophage burst at the exponantial phase of *M. marinum* infection. Double transgenic *Tg(mpeg1:EGFP)* and *Tg(lys:DsRed)* larvae infected with *Mm* were imaged alive every ~63 sec from 1 dpi to 2 dpi by CLSM (Nikon A1). Macrophage burst and spreading of *Mm* (red) are shown, followed by the recruitment of GFP-positive (green) macrophages and DsRed-positive (blue) neutrophils. In the left bottom the macrophages and *Mm* are visualized separately. In the right bottom only the *Mm* are visualized, and the burst event at t = 5h is indicated by arrowheads. A neutrophil phagocytized *Mm* after burst event indicated by an arrow in the upper panel at t= 8 is moving away from the infection site. The maximum intensity projection from 11 CLSM images (step size in z-direction, 5.56 μm) is shown at 10 frames per second. Scale bar: 50 μm.

Video 3. Extrusion of a *M. marinum* aggregate out of the tail fin. Double transgenic *Tg(mpeg1:EGFP)* and *Tg(lys:DsRed)* larvae infected with *M. marinum* were imaged alive every ~60 sec from 1 hpi to 17 hpi by CLSM (Nikon A1). The GFP-positive (green) macrophages containing a *M. marinum* (red) aggregate undergoes cell death showing fragmentation. The bacterial content is clearly extruded from the tail fin 3 hours after the macrophage showing fragmentation (Fig. 3D). The corresponding transmission channel is shown below, showing a protuberance on the outer epithelial layer, which is eventually shed off. The maximum intensity projection from 11 CLSM images (step size in z-direction, 5.56 μm) is shown at 10 frames per second. Scale bar: 20 μm.

Video 4. CLSM on macrophage and neutrophil behavior at the exponantial phase of *M. marinum* infection. Double transgenic *Tg(mpeg1:EGFP)* and *Tg(lys:DsRed)* larvae infected with *M. marinum* were imaged alive every ~60 sec at 3 dpi for 2.5 hours by CLSM (Nikon A1) before fixation. The two infected GFP-positive (green) macrophages and two infected DsRed-positive (blue) neutrophils that were correlated with 3D block-face SEM images are indicated by arrows. The indicated macrophages (MP1 and MP2) phagocytized *Mm* approximately 2 and 1.5 hours before fixation respectively and these cells remained GFP-positive after fixation. The neutrophil (NP1) containing *Mm* was observed 2.5 hours before fixation and undergoes cell death, observed as rapid (within ~1 min) disappearance of the fluorescent signal, ~30 min before fixation. The second neutrophil (NP2) was recruited to another infected neutrophil ~30 min before fixation. The maximum intensity projection from 11 CLSM images (step size in z-direction, 5.56 μm) is shown at 10 frames per second. Scale bar: right panel 100 μm and for the left panel 50 μm.

Video 5. Three-dimensional block-face SEM images of *Mm* infected tail fin. Double transgenic *Tg(mpeg1:EGFP)* and *Tg(lys:DsRed)* larvae infected with *M. marinum* was fixed and block face SEM imaging was performed on an 80 by 80 μm region of interest using a Quanta FEG 250 with a Gatan 3View Ultramicrotome. The video shows 154 images acquired every 150 nm step size in z-direction (103 nm pixel size) at 10 frames per second. Scale Bar: 10 μm.

Video 6. Three-dimensional block-face SEM images of necrotic neutrophil undergoing netosis. Double transgenic *Tg(mpeg1:EGFP)* and *Tg(lys:DsRed)* larva infected with *M. marinum* was fixed and block face SEM imaging was performed on an 80 by 80 μm region of interest using a Quanta FEG 250 with a Gatan 3View Ultramicrotome. The video shows 70 images in z-direction (23 nm pixel size) of the neutrophil (NF2, Fig. 4). Note the partial intact nuclear envelope (arrow) and the vesicles (arrowheads) showing the vesicles fusing with bacterial aggregate. The images were acquired with every 150 nm step size in z-direction and are in this video visualized at 10 frames per second. Scale Bar: 2 μm.